CHEMISTRY & CHEMICAL TECHNOLOGY

Chem. Chem. Technol., 2026, Vol. 20, No. 1, pp. 126–141

Chemical Technology

SYNTHESIS OF NANO COPPER OXIDE FUNCTIONALIZED DATE PITS-DERIVED MICROPOROUS ACTIVATED BIOCHAR AND ITS APPLICATION IN THE ADSORPTIVE DESULFURIZATION OF MODEL AND REAL FUEL OILS

Asmaa N. Al-Irhayim[1], Neam H. Ahmed[2], Neam M.T. Al-Layla[1], Abdelrahman B. Fadhil[1,✉]

[1] Department of Chemistry, College of Science, University of Mosul, Majmoaa str., 41002, Mosul, Iraq
[2] Department of Forensic Evidence, College of Science, University of Mosul, Majmoaa str., 41002, Mosul, Iraq
✉ *abdelrahmanbasil@yahoo.com; abdelrahmanbasil@uomosul.edu.iq*

https://doi.org/10.23939/chcht20.01.126

Abstract. This study explores the synthesis of activated biochar (ABC) from date pits and CuO-ABC nanocomposite for the adsorption elimination (AE) of model and commercial fuels. Outcomes deduced from FESEM, TEM, EDX, XRD, and the N_2 adsorption-desorption isotherms confirmed the microporous structures of both adsorbents. The SA_{BET} as well as pore diameter of the ABC were, respectively, 765.52 m^2/g and 1.79 nm, while the SA_{BET} and pore diameter of CuO-ABC nanocomposite were, respectively, 621.57 m^2/g and 1.99 nm, referring to the micro-porous structures of both adsorbents. The maximum AE % of 200 mg/L DBT solution by the ABC was 98.09 % using 0.20 g of the ABC at 30 °C for 25 min. In comparison, the highest AE % of 200 mg/L DBT solution over the CuO-ABC nanocomposite was 99.24 %, achieved with 0.15 g of nanocomposite at 30 °C for 20 min. The isothermal and kinetic studies revealed that the Langmuir adsorption isotherm and the pseudo-2nd-order kinetic model best described the adsorption of DBT. Both adsorbents exhibited sustained activity across five consecutive cycles. The *S*-content of real gasoline was reduced to 80.12 % and 84.22 % using 0.60 g of both adsorbents at 30 °C for 120 min. This work presents cost-efficient adsorbents for desulfurization of a model desulfurization system and actual fuel oils at the industrial scale.

Keywords: date pits, activated biochar, CuO/ABC nanocomposite, adsorption elimination of DBT, adsorption isotherm and kinetics.

1. Introduction

The extensive utilization of petroleum products has led to significant environmental damage and issues. Industrial processes based on oil derivatives have contaminated the environment and affected human health and other living organisms.[1] Mercaptans, benzothiophene (BT), free sulfur, dibenzothiophene (DBT), disulfides, thiophene (TF), and sulfides are the predominant *S*-containing molecules in petroleum and its fractions.[2] Thiophene and its derivatives (BT and DBT), besides other isomers of DBT, are the predominant *S*-compounds that exert considerable harmful impacts on ecosystems, attributable to their elevated potential for mutation and carcinogenesis.[3] Fuels containing *S*-compounds will produce SO_2 during their combustion, which then reacts with the atmospheric oxygen to produce SO_3. The latter reacts quickly with water vapor to form sulfuric acid, causing serious environmental issues.[4] Corrosion issues and downstream catalysts poisoning are also associated with the utilization of *S*-containing fuels.[5] Accordingly, the quality of the air must be improved as per the Environmental Protection Agency (EPA). To do so, the EPA recommended that the level of *S*-compounds in gasoline must be below 30 ppm and 15 ppm-w for diesel fuel.[6]

In addition to the elevated pressure and temperature required in HDS, this approach cannot eliminate aromatic *S*-compounds, such as benzothiophene (BT), dibenzo-thiophene (DBT), and 4,6-dimethyl DBT.[7,8] Accordingly, alternative desulfurization (DS) approaches have been adopted to diminish *S*-compounds level to a satisfactory threshold to meet regulatory standards, including trans-portation fuels was accomplished by various technologies to eradicate *S*-species, like hydrodesulfurization (HDS), extractive desulfurization (EDS), biodesulfurization (BDS), oxidative desulfurization (ODS), oxidation-extraction desulfurization (OEDS), and adsorptive desulfurization

(ADS).[9,10] The latter has been given increasing concern, as it could achieve the required target at mild temperature and pressure, without any catalysts or oxidants, besides its satisfactory DS efficiency.[11] The ADS is usually conducted employing sorbents of diverse porosity and functionalities to achieve maximum adsorptive capability.[9,12] Solid sorbents of miscellaneous porosity and functionalities have been implemented for deep ADS. In this regard, carbon-based materials, metal oxides, zeolites, MOFs, metal-supported inorganics, and metal-supported carbon have been employed as solid adsorbents in the ADS process.[12]

As a byproduct of biomass carbonization, charcoal has numerous applications beyond its use as a solid fuel. It can also be used to produce gas *via* gasification, as a reductant in metallurgical manufacturing, and for gas purification.[13] Multiple precursors could be implemented in the production of charcoal *via* the slow pyrolysis approach, like wood, agricultural wastes, seeds, *etc.*[14–16] Because activated carbon (AC) or activated biochar (ABC) has an elevated surface area and good porosity, it is among the preferred adsorbents.[17] Moreover, efficient DS of various compounds of sulfur by adsorption can be achieved by using adsorbents with microporosity and varied surface chemistry. Various alterations to AC have been made to increase porosity and surface area.[17] Oxidation or impregnation with metal oxides is among the modification treatments that were tried to enhance the adsorptive capacity of AC to *S*-compounds.[18] Accordingly, modifying the AC *via* impregnating it with various species of metal oxides, like Fe, Co, Ni, and Zr, has been established.[18] Modifying the AC with metal oxides could enhance the adsorptive capacity of AC, as metal oxides have proven their reactivity to *S*-compounds, particularly thiophenes, by forming solid metal thiolates.[18] It was established that modifying adsorbents with metal oxides enhanced the complexation between the thiophene compounds and adsorbent, leading to better elimination of these compounds from fuels, as an outcome of the interaction between the d-electrons in the metal with the empty s-orbital in the compound.[19] So, selecting the proper metal oxide governs the extent of reactivity. For instance, MnO showed better reactivity with *S*-compounds than activated ZnO.[20] Modification of AC with various metals or metal oxides to enhance its adsorptive performance for thiophene compounds has been reported in the literature. The MnO_2-loaded AC created from waste tire rubber (WTR) was tried in the AE of multiple thiophenic compounds from liquid oil *via* the column adsorption route.[19] Danmaliki *et al.*[18] explored the DS of DBT from model oil using a flow system with Ni-modified AC generated from WTR and reported a removal performance of 70 % under typical working conditions. Prajapati and Verma[21] reported supporting carbon nanofibers with Cu/Ni nanoparticles (NPs) for the stripping of thiophene from a model oil in a fixed-bed system. The activated Al_2O_3 loaded with ZnO was tested for the DS of jet fuel *via* adsorption-assisted ultrasonication.[22] Nazal *et al.*[23] investigated the AE of DBT from model diesel ADS over the Al_2O_3/AC adsorbent and reported an adsorptive capacity of 85.0 mg/g. Synthesis of Ag/ZSM-5 zeolite was accomplished by Xiao *et al.*[24] The resultant adsorbent was employed in the ADS of thiophene from model gasoline with an adsorptive capacity of 0.213 mmol S/g. Lastly, CuO-Mn/AC was used to remove DBT from the model gasoline, achieving 91.10 % efficiency.[25] Nonetheless, synthesis of ABC from date pits (DPs) as a potential precursor *via* a two-step route, namely carbonization-KOH activation, has not been declared in the literature, as far as we know. Moreover, exploiting the resulting ABC as an adsorbent for eliminating DBT from model oil, as well as using it to create a copper oxide / AC nanocomposite (CuO/AC-ACNC) for the same purpose, has not been explored, as far as we know. Additionally, testing the as-prepared ABC and its derived nanocomposite in the DS of real gasoline fuel, and comparing the results with those of model oil. All these goals motivated us to complete this study and fill this gap.

In this context, the development of a microporous ABC from DPs by the carbonization-KOH activation route, followed by mixing the as-prepared ABC with $CuCl_2$ to produce a CuO-ABC nanocomposite. The original ABC, in addition to its prepared nanocomposite, was characterized by numerous methods to assess its texture, morphological, and physicochemical characteristics, and then tested for stripping DBT from a model fuel and *S*-species from actual gasoline. The DBT adsorption kinetics and isotherms by the adsorbents were also investigated. Lastly, the ability to reuse spent adsorbents was also explored.

2. Experimental

2.1. Chemicals and Precursors

Dibenzothiophene (DBT, 98 %) was obtained from Sigma Aldrich, while *n*-hexane (99.0 %), potassium hydroxide (KOH, pellets, 98.0 %), and copper chloride dihydrate ($CuCl_2{\cdot}2H_2O$, 99.0 %) were purchased from Scharlau Chemicals, Spain. These chemicals were employed as bought without any pre-treatment. The DPs were stripped from the date palm fruit and used to create the ABC.

2.1.1. Synthesis of ABC from DPs

A double-step process, carbonization-activation, was applied to create the AC. First, the DPs were rinsed with hot distilled water (DW) to eradicate dirt and other impurities. After drying for 10 h at 105 °C, the DPs were pulverized and sieved through a 100-mesh sieve. The

obtained particles were then carbonized at 450 °C for 1h in a fixed-bed reactor under a stream of inert N_2 gas, with a 30 °C/min rate of heating. The produced biochar (BC) was then crushed and screened to acquire particles of 100-mesh size. A specific mass of the resulting BC was mixed with the activator (KOH) pellets at a mass ratio of 2:1 KOH: BC. Next, DW was added to dissolve the KOH, and the resultant mixture was stirred for 5 h and left overnight. Next, the mixture was dehydrated at 105 °C until dry. Afterwards, the dried mixture was thermally treated in a muffle furnace (Isolab, Germany) to initiate the chemical activation by KOH. The activation was performed at 750 °C for 90 minutes, with a heating rate of 10 °C/min.[21] The produced ABC was then immersed in a 1M solution of HCl for a day to get rid of any inorganic salts, followed by successive washing by hot DW till a neutral pH was reached. Subsequently, the ABC was desiccated at 105 °C for 10 h and then sieved through a 100-mesh sieve to obtain homogeneous ABC particles. Lastly, the ABC was preserved in an air-tight container for identification and use.[26,27]

2.1.2. Synthesis of CuO/ABC Nanocomposite

The ABC was synthesized from the DPs *via* KOH activation to produce the CuO/ABC nanocomposite. Firstly, a given quantity of the ABC (5.0 g) was submerged in solutions comprising diverse concentrations of Cu (2.5–10.0 % w/w), which was quantified by implementing $CuCl_2{\cdot}2H_2O$ as a precursor for Cu. The resulting mixtures were stirred for 5h and left overnight to ensure proper loading of Cu on the ABC surface. Afterwards, the impregnated samples were desiccated at 105 °C for 10 h. The CuO/ABC nanocomposite was synthesized by thermal calcination of the dried samples. Accordingly, the treated samples were calcinated at various temperatures (300–600 °C) for multiple durations (60, 90, 120, and 150 min) to select the optimal composite. The composite was selected based on the adsorptive performance of DBT from model oil using the prepared samples. Each experiment was repeated in duplicate, and the recorded outcomes represent the average ±SD.

2.1.3. Characterization of ABC and CuO/ABC Nanocomposite

The ABC and its derived nanocomposite were characterized using multiple techniques. A Fourier transform Infrared (FTIR) spectrophotometer (Shimadzu 1800, Japan) was used to inspect the surface functionalities of the AC and CuO/AC adsorbents. The surface morphology and elemental composition of both adsorbents were specified by Field Emission Scanning Electron Microscopy (FESEM) coupled with Energy Dispersive X-ray (EDX) spectroscopy. Porosity, in addition to surface texture, of both AC and the CuO/AC nanocomposite was measured using a surface area analyzer. The specific surface area and pore-size distribution of the adsorbents were determined from N_2 adsorption-desorption isotherms. X-ray diffraction (PANalytical, EMPYREAN, Netherlands) was employed to characterize the crystalline composition of the ABC and its generated CuO/ABC nanocomposite at a 2°/min scanning rate over the 10–80° diffraction angle range. The transmission electron microscopy (TEM) of the adsorbent surfaces was also determined using a FEI Tecnai G2 F20 S-Twin TEM analyzer to examine the microstructure of the resulting adsorbents.

2.2. Methods

2.2.1. Adsorption Experiments

The DBT adsorption trials over the ABC and CuO/AC nanocomposite were carried out *via* the optimized methodology. Variables affecting the eradication performance of DBT by the as-created adsorbents were optimized. These variables included the amount of the adsorbents implemented (0.05–0.30 g), adsorption temperature (10–60 °C), adsorption interval (5–30 min), and the initial concentration of the adsorbate (DBT, 50–300 mg/L). The optimization was achieved by varying one variable while keeping the others fixed. In a distinctive trial, a quantified mass of each adsorbent was added to 25 mL of the model oil (200 mg/L DBT in n-hexane) in a conical flask. The flask was then shaken on a temperature-controlled shaker at 600 rpm for the specified duration. A standard calibration curve was prepared from a stock solution to determine the residual DBT concentration in the model oil by measuring absorbance at 325 nm on a UV-1900i Spectrophotometer (Shimadzu, Japan).[26] Each adsorption run was conducted twice, and the recorded value represents the mean ±SD. The amount of DBT adsorbed per unit mass of the adsorbent (mg/g), as well as the percentage of the *ADS*, were specified following Eq. (1) and Eq. (2), respectively.

$$q_e\ (\mathrm{mg/g}) = \frac{(C_\mathrm{o} - C_e)\,V}{m} \qquad (1)$$

$$ADS\ (\%) = \frac{(C_\mathrm{o} - C_e)}{C_0} \times 100 \qquad (2)$$

where C_o (DBT initial concentration) and C_e (DBT equilibrium concentration (mg/L), while V and m refer respectively to the volume of DBT solution used (L) and the quantity of the adsorbent (g).

2.2.2. Isothermal and Kinetics of DBT Adsorption

Exploring DBT sorption isotherms by the ABC and its resultant nanocomposite was accomplished by mixing

25 mL of DBT solutions with diverse concentrations (25–300 mg/L) with a given quantity of the adsorbent in a 250 mL round-bottom flask. The mixtures were shaken at 400 rpm on a temperature-controlled shaker for the specified duration at the optimal temperature. At equilibrium, the adsorbent was stripped from the solutions, and the residual DBT concentration was measured. To ensure reproducibility, each experiment was performed at least twice, and the reported value represents the average ±SD. The obtained outcomes were analyzed using the Langmuir and the Freundlich adsorption isotherms, whose nonlinear forms are presented in Table 1.

Table 1. Models of isotherms implemented in analyzing DBT adsorption outcomes

Model of isotherm	Non-linear form	Description of parameters
Langmuir	$q_e = \frac{K_L C_e}{1 + K_L\, C_e}$	C_e (mg/L): DBT concentration at equilibrium. q_e (mg/g): amount of DBT eliminated at equilibrium. q_e (mg/g): amount of DBT eliminated at equilibrium. K_L (L/mg): the Langmuir constant
Freundlich	$q_e = K_F C_e^{1/n}$	C_e (mg/L): DBT concentration at equilibrium. q_e (mg/g): amount of DBT eliminated at equilibrium. K_F (mg/g): DBT adsorption capacity. n: heterogeneity factor
Pseudo-1st-order	$q_t = q_t - e^{-k1t}$	q_t (mg/g): Amount of DBT eliminated at time (t). q_e (mg/g): Amount of DBT eliminated at equilibrium. k_1 (1/min): rate constant of the pseudo-2nd-order
Pseudo- 2nd -order	$q_t = \frac{k_2 {q_e}^2}{1 + k_2\, q_e t}$	q_t (mg/g): Amount of DBT eliminated at time (t). q_e (mg/g): Amount of DBT eliminated at equilibrium. k_2 (g/mg min): rate constant of the pseudo-2nd-order
Intra-particle diffusion	$q_t = K_{id}\, t^{0.5} + C$	q_t (mg/g): Amount of DBT eliminated at time (t). K_{id} (mg/g min$^{0.5}$): intra-particle diffusion rate constant. C (mg/g): A constant shows the thickness of the boundary layer

To investigate DBT kinetics of adsorption, a proper weight of the adsorbent (AC or CuO/ABC) was mixed with a 25 mL DBT solution (200 mg/L). The resultant blend was shaken at a definite temperature for numerous durations. Quantifying the adsorption amount was made by determining the concentration of DBT at 5–120-minute intervals. The pseudo-1st-order (PFO), pseudo-2nd-order (PSO), and intra-particle diffusion (IPD) models were applied to analyze the adsorption data. Table 1 lists the non-linear forms of these models.

2.2.3. Regeneration of Spent Adsorbents

The ABC or CuO/AC adsorbents were regenerated after DBT adsorption in a Soxhlet apparatus using a suitable solvent (*n*-hexane). The consumed specimens were placed into the extractor, and the adsorbed DBT was stripped for 4 h. After DBT desorption, a portion of the renewed adsorbents was dried at 105 °C for 5h in an oven, then heated at 500 °C for 30 min.[2] Five rejuvenation series were performed. In each, the process was carried out at the best typical settings to achieve the maximum eradication of DBT from oil. Each reusability experiment was repeated twice, and the values were presented as the mean ±SD.

3. Results and Discussions

3.1. Synthesis of CuO/ABC Nanocomposite

The CuO/AC composite was prepared from the as-developed ABC using the optimized methodology. Accordingly, multiple experiments were conducted to optimize the amount of Cu loaded onto the ABC (2.5–10.0 wt. %), the calcination temperature (300–600 °C), and the calcination period (0.50–2.0 h). Selecting the typical composite was based on the ability of the produced CuO/AC composite samples to achieve the maximum AE of DBT in oil under the conditions shown in the legend of Fig. 1, *a–c*.

The findings in Fig. 1, *a* show that the highest AE % of DBT in the oil was achieved when the Cu overfill on the ABC increased from 2.5 wt. % to 5.0 wt. %. The increase in the number of active sites contributing to DBT adsorption could be behind this enhancement in the AE performance of DBT from the fuel.[25] When the quantity of Cu supported on the ABC increased beyond 5.0 wt. %, a decrease in the AE % of DBT was observed, as a consequence of CuO particle assemblage, which in turn lessened many energetic positions contributing to eradicating DBT from oil.[25]

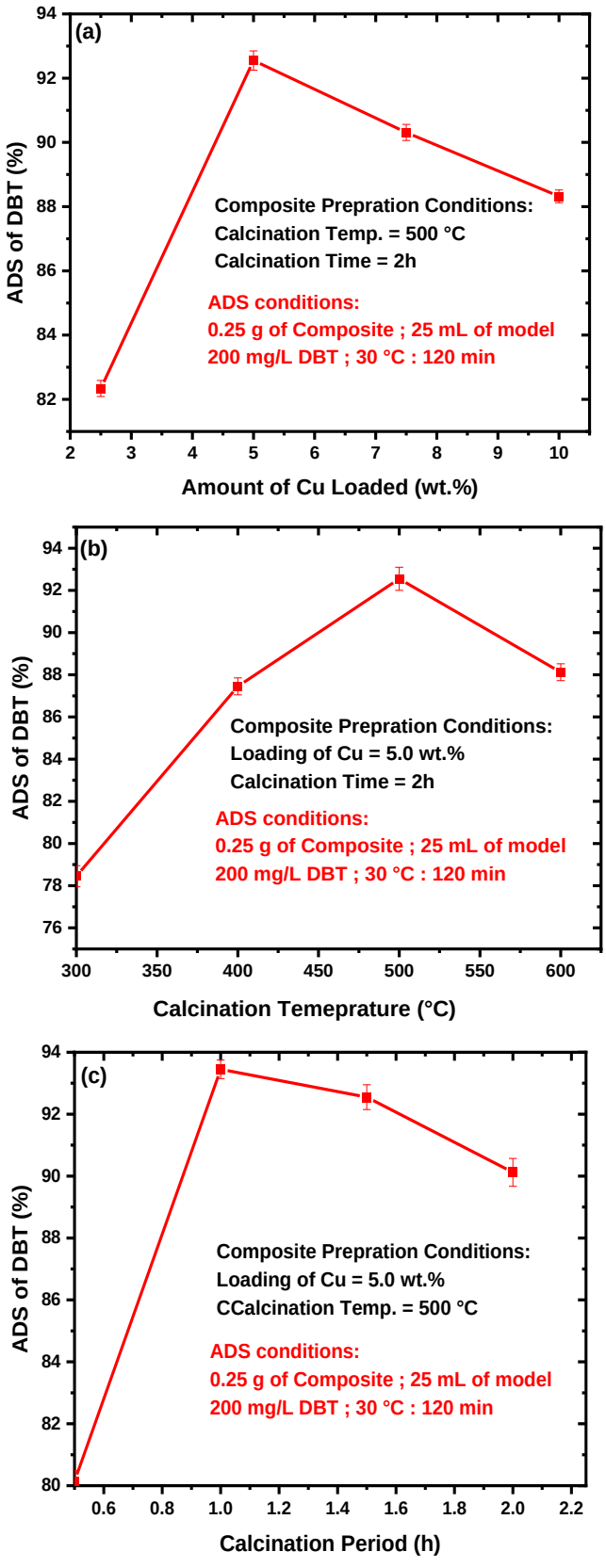

Fig. 1. Optimization of synthesis variables to select the optimal nanocomposite

Among the factors that were optimized upon the preparation of the CuO/AC composite was the influence of the calcination temperature, which was studied over a range of temperatures (300–600 °C). As offered in Fig. 1, *b*, increasing the calcination temperature led to a higher AE % of DBT, as an outcome of the creation of additional active sites. A calcination temperature of 500 °C achieved the highest AE % of DBT from oil. At the same time, above 500 °C, the adsorptive ability of the produced composite diminished, owing to the sintering of the composite, which originated from the gathering of CuO particles with each other, resulting in a minimization in the number of viable positions taking part in the removal of DBT from oil.[25]

The calcination period was among the conditions optimized during preparation of the CuO/AC composite. Fig. 1, *c*, which offers the influence of the calcination time (0.50–2.0 h) on the AE % of DBT by the synthesized adsorbents, shows that the AE % improved when the time of calcination extended from 0.50 h to 1.0 h, while a decrease in the AE % occurred as the time extended to 1.0 h. Sintering of the CuO particles could be responsible for reducing the AE performance of DBT in the fuel after 1 h.[20] Based on the above outcomes, the typical CuO/AC composite synthesized by loading 5.0 wt. % of Cu and calcined at 500 °C for 1 h was typical. Correspondingly, it will be employed in the subsequent trials of DBT elimination from both fuels (model and real).

3.2. Identification of ABC and CuO/ABC Nanocomposite

Multiple techniques were implemented to characterize the ABC and its optimal composite. The SA_{BET}, pore volume, and mean pore diameter of the as-developed ABC and CuO/ABC composite were specified as per the N_2 adsorption-desorption isotherms, which are offered in Fig. 2.

It was found that the developed ABC disclosed a typical type-I isotherm according to IUPAC, indicating a predominance of micropores.[28] In this type, capillary condensation in micropores of the authentic ABC causes the N_2 adsorption-desorption isotherms to rise rapidly at a lower relative pressure (P/P_0 = 0.01). Regarding the CuO/ABC composite, the N_2 adsorption-desorption isotherm of this adsorbent demonstrated a hybrid isotherm, specifically type-I at low relative pressures and type-IV at medium and elevated relative pressures.[28] At the low P/P_0 region, N_2 adsorption was quick, and no plateau appeared at medium relative pressures. Moreover, a notable hysteresis loop was observed in the medium-pressure range ($0.45 < P/P_0 < 0.95$), indicating the presence of mesopores alongside micropores in these materials.[28] Also, a notable hysteresis loop (Type H4) suggested that this adsorbent contains slit-shaped pores and mesopores.[29]

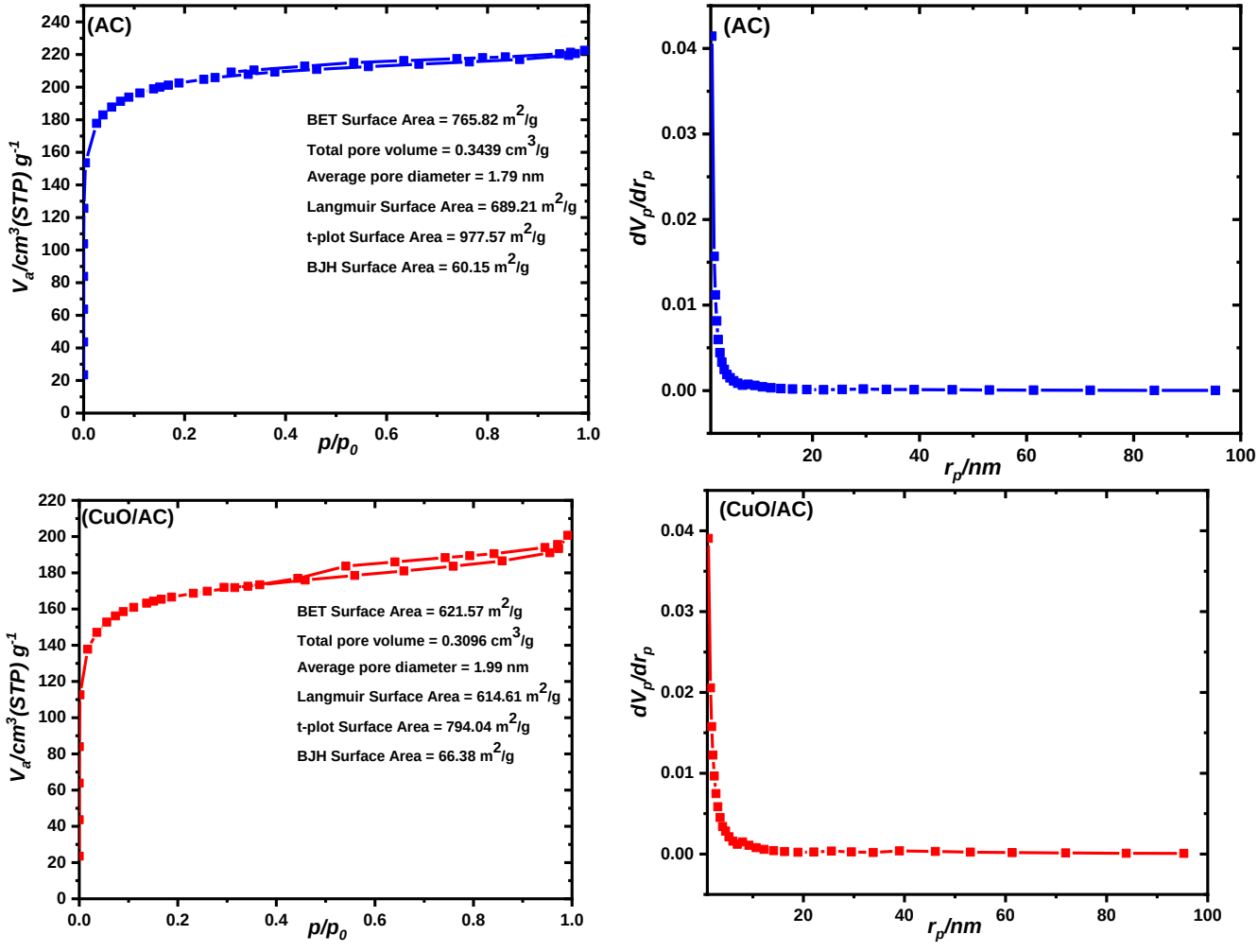

Fig. 2. Adsorption-desorption isotherms N_2 gas and the pore size distributions of the ABC and CuO/ABC nanocomposite

The ABC possessed a SA_{BET} of 765.52 m^2/g, whereas its pore volume was 0.3439 cm^3/g. After incorporating CuO onto the ABC surface, the SA_{BET} diminished to 621.57 m^2/g, and the pore volume decreased to 0.3096 cm^3/g. Moreover, the average pore diameter and the ABC's mesopores surface (BJH) were 1.79 nm and 60.15 m^2/g, respectively. However, after CuO loading on the ABC surface, the average pore diameter and the BJH surface area rose, respectively, to 1.99 nm and 66.38 m^2/g. Such a finding could be ascribed to the increase in mesopore content after CuO loading, which originated from the composite during heat treatment. Similar findings were also reported by Prajapati and Verma[29] and Fayazi and Ghanei-Motlagh[30] upon loading NiO and Cu (II) on the AC developed from various precursors.

Examining the crystal structures of the authentic ABC and its developed nanocomposite was accomplished using XRD. The XRD patterns of the ABC and its derived adsorbent (Fig. 3) showed two broad distinguishing peaks at $2\theta = 25.2°$ and 43.5°, indicating the amorphous (002) and graphitic (100) carbon of the ABC.[30,31] At the same time, the XRD patterns of the CuO/ABC nanocomposite showed additional peaks belonging to the crystalline planes of CuO. These peaks were detected at $2\theta = 35.5°$, 38.6°, and 61.5° and correspond to the phases (111), (111), and (113), respectively, demonstrating that CuO was successfully loaded on the surface of the produced ABC.[29] The above crystalline planes of CuO were also detected upon loading CuO on the surfaces of different commercial ABC samples.[29] Calculating the crystalline size diameter (D) of the CuO/ABC nanocomposite was carried out following the Debye-Scherrer equation, and the results exhibited that the values of D were between 21.51 nm and 46.27 nm. The average size of the CuO/ABC nanocomposite crystalline structure, computed based on the Scherrer equation, was 25.37 nm. These observations certified the nanoscale structure of the as-synthesized nanocomposite.

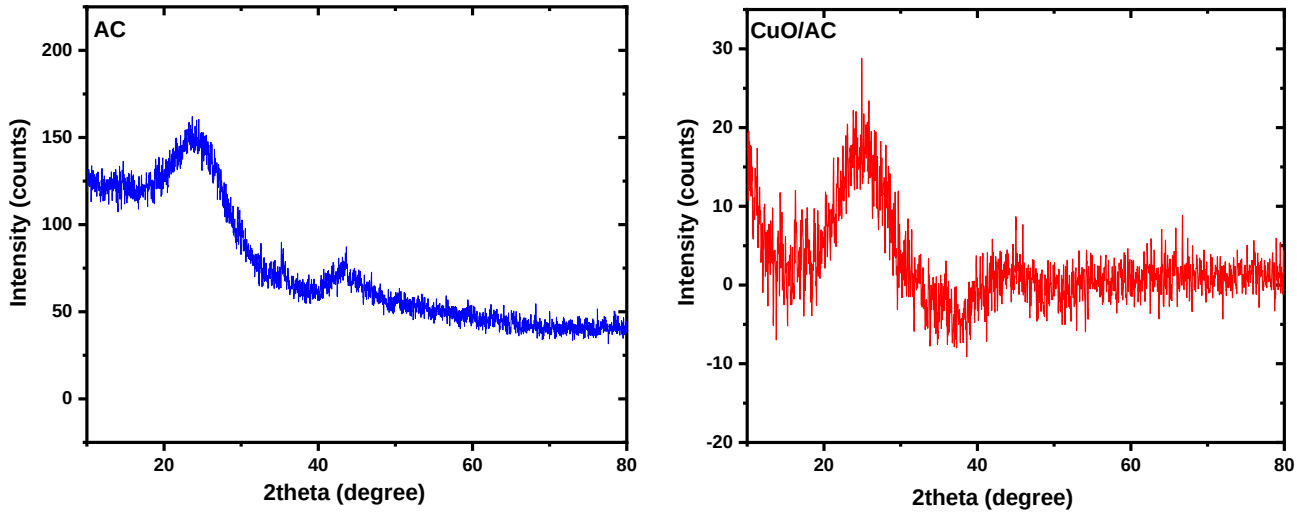

Fig. 3. XRD patterns of the ABC and its CuO/ABC nanocomposite

The morphological characteristics of the pristine ABC and its derived nanocomposite were examined using FE-SEM. According to Fig. 4, which displays FESEM images besides EDX elemental distribution of the authentic ABC, the latter's surface contained numerous pores and openings of various shapes and sizes. Also, these pores and openings were irregular in shape and size. On the other hand, the EDX mapping of the authentic ABC disclosed that C was mainly formed of C (92.20 %), O (7.50 %), and K (0.30 %). The low K concentration confirmed that the activator (KOH) was completely consumed during the transformation of the parent BC into ABC.

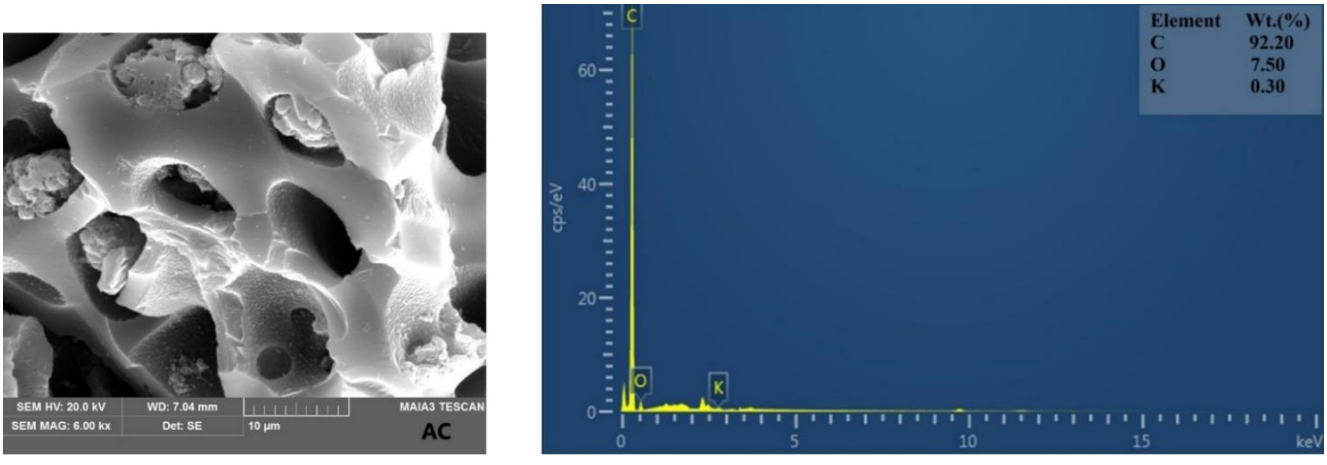

Fig. 4. FE-SEM images of EDX mapping of the ABC

FESEM image of the CuO/ABC nanocomposite is illustrated in Fig. 5. It shows that after loading CuO on the surface of the created ABC, followed by calcination, no significant difference in the surface morphology of the ABC occurred, indicating that the essential composition of the pristine ABC was not destroyed. However, FESEM images of the CuO/ABC nanocomposite revealed a spherical particle distribution on the surface, indicating successful CuO loading. Based on the EDX analysis, the CuO nanocomposite contained, in addition to C and O, 3.90 wt. % Cu. These outcomes also confirm that CuO was formed and loaded onto the ABC, aligning with findings from BET, FESEM, and XRD measurements.

TEM analysis was accomplished to recognize the size and shape of the CuO/ABC nanocomposite produced. Fig. 6, which depicts TEM images of the as-developed composite, revealed that Cu occurs as nanoparticles or clusters. It can be observed that the CuO nanoparticles are mostly spherical, and the most intense dark bands correspond to agglomerates of these particles. Also, from

TEM images, the average diameter of the CuO NPs was below 100 nm, consistent with the XRD measurements, which reported an average size of 25.37 nm.

3.3. Optimization of DBT Elimination Parameters

The elimination of DBT from model oil was investigated by optimizing variables to achieve the maximum AE %, as follows:

3.3.1. Effect of the Dosage of the Adsorbent

Examining the impact of the adsorbent dosage on the AE % of DBT by the ABC and CuO/ABC nanocomposite under the experimental conditions presented in Fig. 7 was accomplished by trying multiple amounts of both adsorbents (0.05–0.30 g). It was observed that the AE % of DBT improved from 80.08 % to 97.19 % when the ABC dosage increased from 0.05 g to 0.20 g, and from 86.68 % to 99.08 % when the mass of CuO/ABC increased from 0.05 g to 0.15 g. Typically, higher dosages increase the availability of active adsorption positions on the absorbent surface, thereby improving the AE %.[32,33] The adsorption system was unable to achieve complete removal due to competitive adsorption of DBT species onto the adsorbents, as well as the presence of an adsorption-desorption equilibrium. Conversely, the reduction in DBT adsorption ability with increasing adsorbent dosage may be ascribed to several factors, including, at low adsorbent concentrations in the solution, the competition between DBT molecules for the active adsorption sites of the ABC and CuO/ABC nanocomposite, resulting in elevated adsorption performance.[34] At the same time, adsorbent aggregation may have occurred at the elevated dosages within the specified volume of solution, diminishing the accessible active sites available for the adsorption of DBT species and hence limiting the AE % of DBT.[35] The higher eradication of DBT by the CuO/ABC nanocomposite than its original ABC might be attributed to the availability of more active sites on its surface than those of the ABC. These positions will increase interaction with DBT species, thereby improving pollutant removal from the oil.

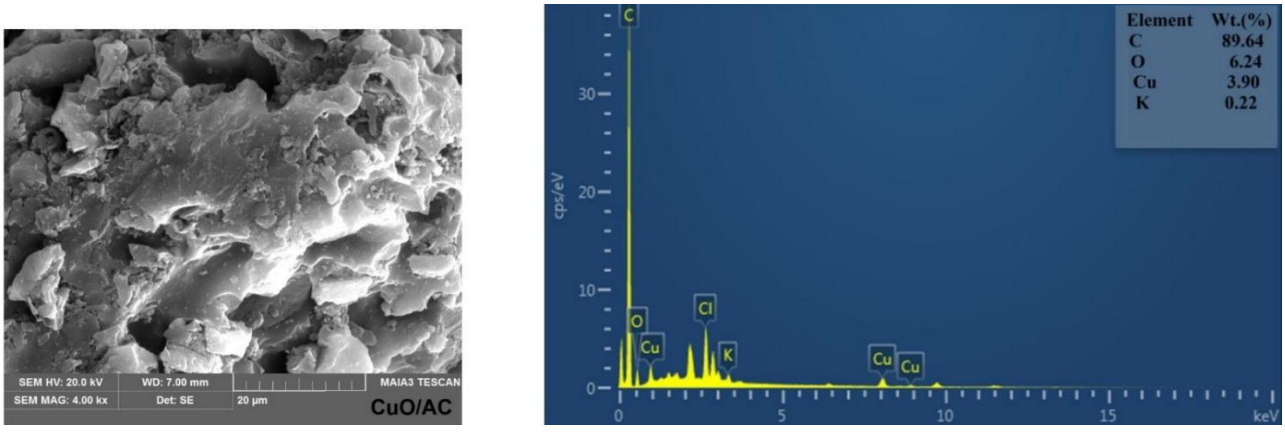

Fig. 5. FESEM images and ED mapping of CuO/ABC nanocomposite

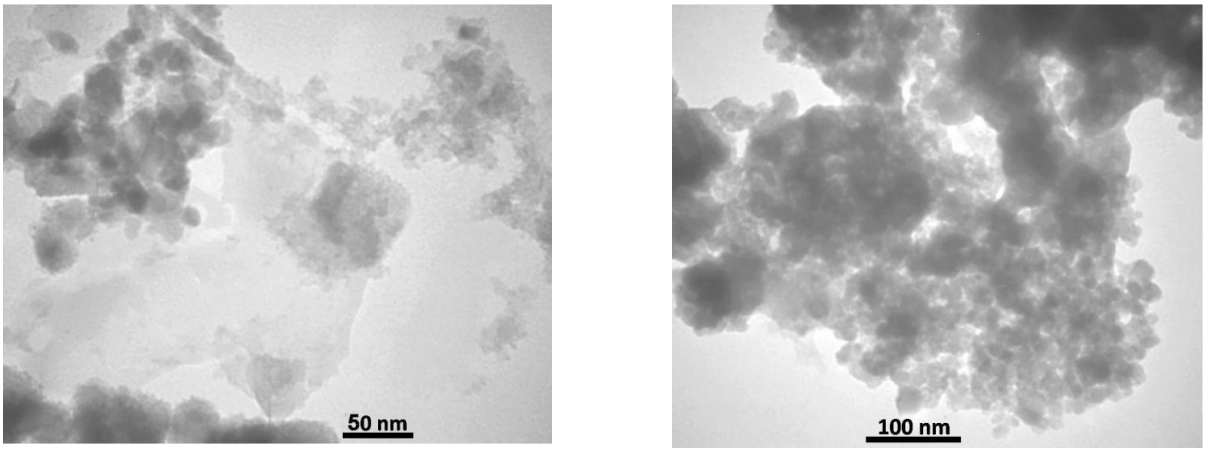

Fig. 6. TEM images of the CuO/ABC nanocomposite

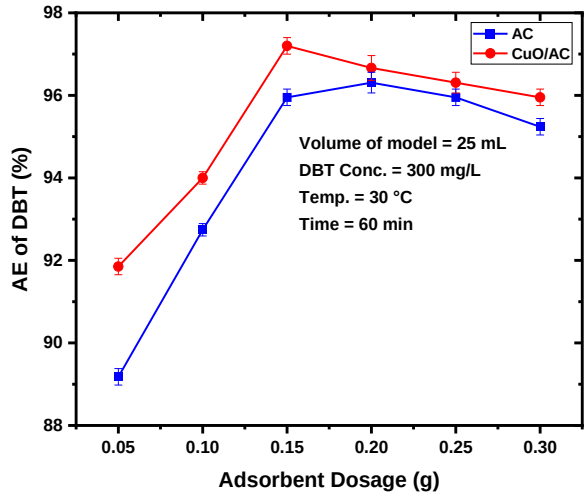

Fig. 7. Impact of the dosage of the ABC or nanocomposite on the AE % of DBT

3.3.2. Effect of the AE Temperature

Fig. 8 demonstrates the impact of temperature on DBT exclusion over both adsorbents, examined across several solution temperatures (10–60 °C) while retaining auxiliary conditions unchanged.

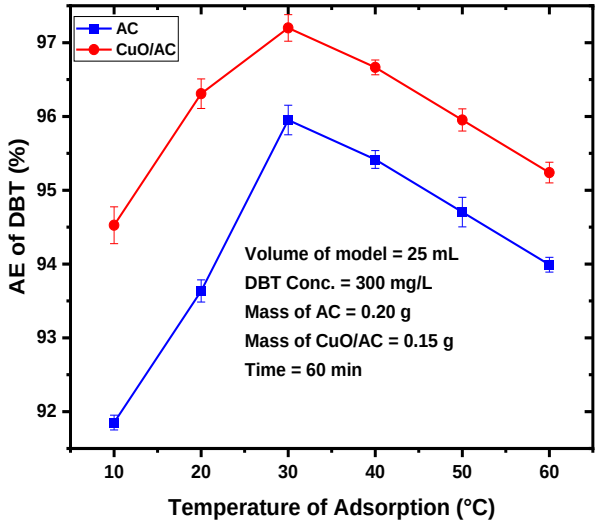

Fig. 8. Impact of the adsorption temperature on DBT elimination

According to the outcomes offered in this figure, raising the temperature from 10 °C to 30 °C (ambient temperature) increased the AE %. These consequences imply that the adsorption process is endothermic. Such observations can be attributed to the increase in solution temperature, which increases the accessibility of surface-active sites and reduces the diffusion resistance of DBT into the nanocomposite, thereby promoting its adsorption.[36,37] Nonetheless, the drop in the AE % when the temperature exceeded 30 °C was ascribed to the rise in the system's molecular kinetic energy, which subsequently diminished DBT with the vigorous positions of the adsorbent.[5] It is worth noting that achieving superlative DBT removal at low temperatures (ambient) will be beneficial for industrial applications.

3.3.3. Effect of the AE Period

The duration of contact between the sorbent particles and the adsorbate species is crucial in the adsorption process. Therefore, the impact of this factor was inspected during the adsorption of DBT on ABC and the CuO/ABC nanocomposite at various contact times (5–30 min), while keeping other parameters fixed, as depicted in Fig. 9.

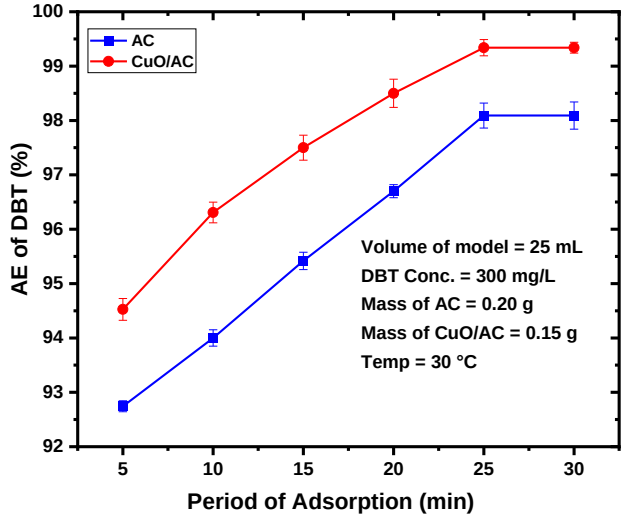

Fig. 9. Effect of the adsorption period on the AE % of DBT

Based on the findings illustrated in this figure, the AE % of DBT from the oil exceeded 92.0 % within 5 minutes of contact, and the removal was enhanced, reaching a maximum at 25 minutes with both adsorbents. The rapid adsorption of DBT onto the ABC and the CuO/ABC nanocomposite in the initial stages of adsorption might belong to diverse factors, including the presence of active sites, the strong concentration gradient of DBT, and the adsorption energy of the adsorbents and their porous structures. Periods above the typical values did not influence the AE performance. Achieving the maximum AE % of DBT from the oil encourages the adoption of the prepared adsorbents for industrial-scale application.

3.3.4. Effect of DBT Concentration

Using the conditions presented in Fig. 10, the impact of trying solutions containing multiple initial concentrations of DBT (25–300 mg/L) on the AE % over the AC and CuO/AC nanocomposite was examined. A drop in the AE % of DBT was observed as the DBT concentration increased from 25 mg/L to 300 mg/L. Such an outcome results from the generally acknowledged fact that, with an increased concentration of DBT solution, a considerable amount of adsorbate competes for available active sites, thus causing a drastic drop in the AE %.[38] Furthermore, the quantity of accessible active sites diminishes with the continued development of adsorption, which causes a decline in AE % of DBT species at elevated concentrations.[2] Similar outcomes were reported for the AE % of DBT across numerous models of fuel using different adsorbents.[2,4,16,35] Conversely, the DBT adsorption capacity (mg/g) was developed when the DBT concentration rose from 25 mg/L to 300 mg/L due to the elevated concentration of DBT substantially enhancing the driving force necessary to efficiently surmount the resistance to the mass transfer process from the solid phase to the liquid solution, consequently augmenting the adsorption capacity of DBT.[39]

3.4. Evaluation of Adsorption Isotherms

When the concentration of the adsorbate is constant, the adsorption equilibrium study explains how the adsorbate is distributed between the solid adsorbent and the liquid solution.[40] In the current investigation, the well-known equilibrium adsorption isotherms, namely the Langmuir and the Freundlich, were explored to deduce information on the adsorption mechanism and the maximum adsorption capacity (q_{max}) of the adsorbent.

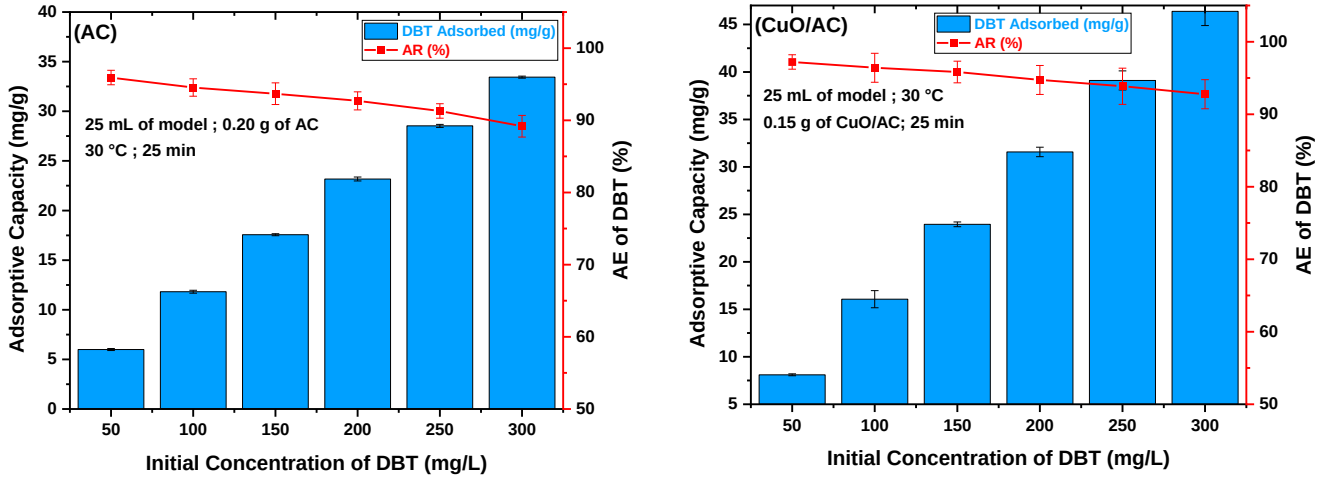

Fig. 10. Effect of DBT initial concentration on its AE % and q_e of adsorbents

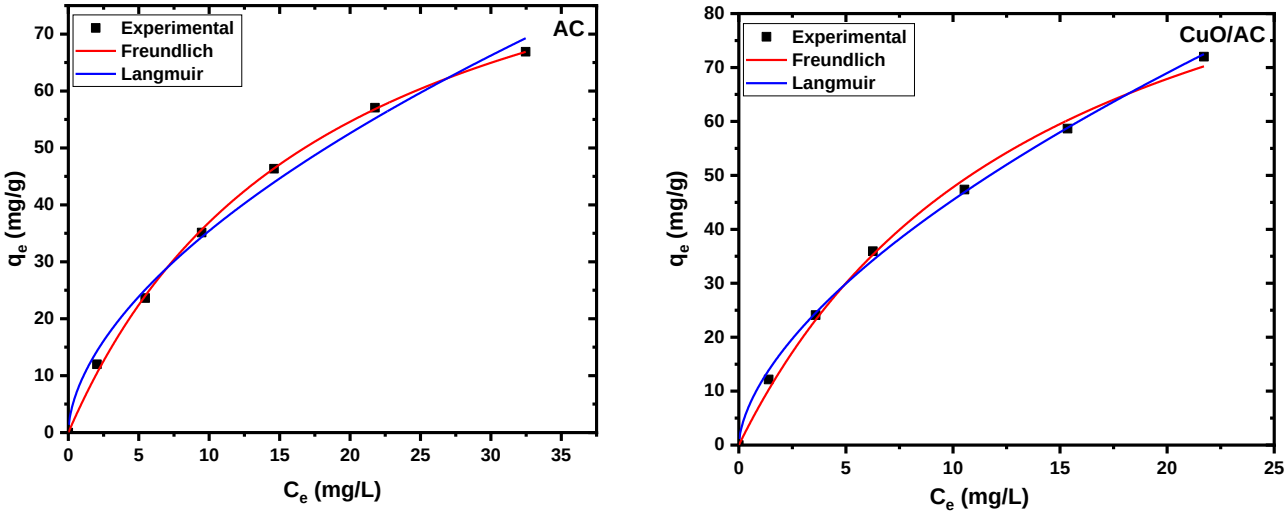

Fig. 11. Adsorption isotherms of DBT over the as-developed adsorbents

Constants relating to the non-linear adsorption isotherms for DBT adsorption over the ABC and its derived nanocomposite are presented in Table 1, while their plots are displayed in Fig. 11. From the non-linear plot of C_e *vs.* q_e, constants relating to the Langmuir isotherm (q_{max} and K_L) and the Freundlich isotherm (n and K_F) could be obtained. The Langmuir adsorption isotherm presumes monolayer adsorption on a uniform surface.[2,4] The adsorption viability can be assessed from the dimensionless equilibrium parameter (R_L). The value of R_L is between 0.0 and 1.0. Based on the R_L value, the adsorption could be preferable ($0 < R_L < 1$), irreversible ($R_L = 0$), unfavorable ($R_L > 0$), or linear ($R_L = 1$).[35] The Freundlich isotherm involves multilayer adsorption on heterogeneous surfaces. The Freundlich constants K_F and n, respectively, represent adsorption capacity and adsorption intensity.[35] According to this isotherm, adsorption is preferred when $n = 1.0$.

The values of correlation coefficient (R^2), q_{max}, K_L, R_L, n, and K_F are tabulated in Table 2. The values of R_L for DBT adsorption by the ABC and CuO/ABC were respectively 0.0546 and 0.0462. Both values were above 0.0 and below 1.0. Consequently, the adsorption of DBT by the adsorbents following the Langmuir isotherm is preferable. On the other side, values of n for DBT adsorption by the AC and CuO/ABC were respectively 1.75 and 1.64. Both values were above 1.0; thus, DBT adsorption over the ABC and its developed nanocomposite was favorable. Based on R^2 values, the Langmuir isotherm provided a superior fit compared to the Freundlich and Temkin isotherms for DBT adsorption over the said adsorbents. Additionally, the theoretical adsorption capacity values were closer to the experimental outcomes following the Langmuir model. These findings demonstrated that the AC and CuO/AC surfaces were responsible for the homogeneous monolayer adsorption of DBT. Additionally, no transmigration of adsorbed DBT molecules occurred due to specific adsorption sites.[30] The adsorption of DBT from the model oil over copper (II)-alginate beads also indicated that the Langmuir model best fit the adsorption data.[30]

Table 2. Adsorption isotherm constants for DBT over ABC and CuO/ABC nanocomposite

AC						
Langmuir isotherm				Freundlich isotherm		
R^2	Q_m, mg/g	K_L, L/mg	R_L	R^2	K_F, (mg/g)/(mg/L)1/n	n
0.9992	104.58	0.0546	0.0575	0.9891	9.55	1.78
CuO/AC nanocomposite						
				Freundlich isotherm		
R^2	Q_m, mg/g	K_L, L/mg	R_L	R^2	K_F, mg/g)/(mg/L)1/n	n
0.9974	117.17	0.0688	0.0509	0.9899	11.34	1.66

3.5. DBT Adsorption Kinetics

The mass transfer of adsorbate from the liquid phase to the solid surface of the adsorbent can be better understood through kinetic studies of adsorption.[40,41] So, the kinetic parameters of DBT adsorption by the ABC and its derived nanocomposite were determined by measuring DBT elimination from both adsorbents over varying time intervals using a 300 mg/L DBT solution and the typical amounts of each adsorbent at 30 °C. The experimental data gathered were plotted for several kinetic models, including PFO, PSO, and IPD, as illustrated in Table 3, while their non-linear plots are offered in Fig. 12.

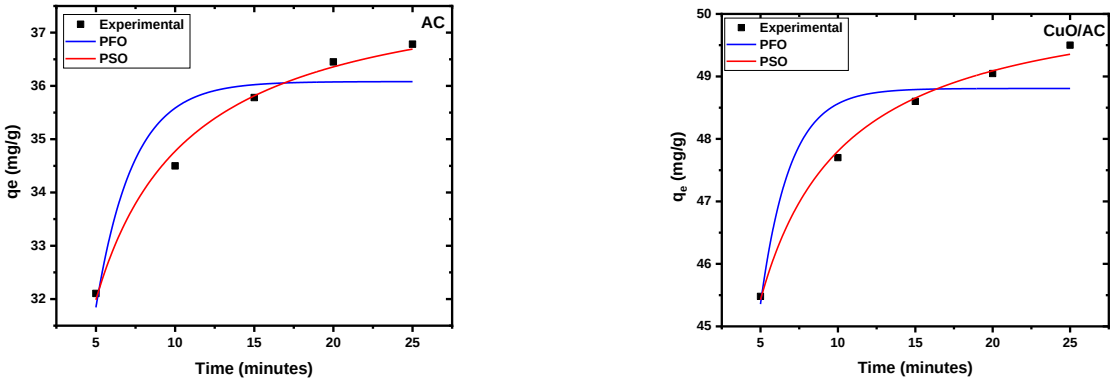

Fig. 12. Adsorption kinetics of DBT over the as-developed adsorbents

The optimal model was determined by assessing its dependability in representing the experimental q_e values and R^2. Compared to the PFO model, the PSO model yields a correlation factor (R^2) near 1.0, indicating that the SBT adsorption kinetics on both adsorbents best fit the PSO model (Table 3). Conversely, the R^2 for the PFO was significantly below 1.0, indicating its unsuitability to express the adsorption of DBT by the prepared adsorbents. Accordingly, chemisorption, which involves valence forces through the sharing or exchange of electrons between the adsorbent surface and adsorbate molecules, predominates during the adsorption process of DBT onto the AC and CuO/ABC nanocomposite. These findings are consistent with those reported for stripping DBT from diverse liquid oil models using multiple adsorbents.[2,4,30,40]

Table 3. The adsorption kinetics model the constants of DBT over ABC and CuO/ABC nanocomposite

ABC								
PFO			PSO			IPD		
R^2	q_t, mg/g	k_1, L/mg	R^2	q_t, mg/g	k_2, L/mg	R^2	K_{diff}	C
0.8659	34.08	0.4283	0.9926	38.09	0.0275	0.8089	7.16	6.90
CuO/ABC nanocomposite								
PFO			PSO			IPD		
R^2	q_t, mg/g	k_1, L/mg	R^2	q_t, mg/g	k_2, L/mg	R^2	K_{diff}	C
0.8681	45.80	0.5298	0.9960	50.44	0.0375	0.7726	9.50	10.26

Regarding the IPD model, it was noted that the IPD line for adsorbing DBT over both adsorbents did not pass through the origin, suggesting that IPD is not the sole rate-regulatory factor in the adsorption process.[4,35,40]

3.6. The DS of commercial fuel

The current study also explored the AE of real gasoline using the as-developed adsorbents, optimizing the effects of adsorbent mass, AE temperature, and AE period on elimination performance, as presented in Fig. 13, *a–c*.

Fig. 13, *a* clearly illustrates that process performance improves as the dosage of adsorbents used to eliminate *S*-compounds in real gasoline increases. This result indicates that increasing the quantity of adsorbents employed will increase the number of adsorbent particles and the beneficial positions, thereby improving AE %.[2,4] It was noticed that using 0.75 g of the ABC compared with 0.60 g of the CuO/ABC nanocomposite. On the other hand, the effectiveness of S-compound removal from gasoline decreased as the optimal dosage increased. This could be because the adsorbent particles accumulate, reducing the number of particles and the number of effective adsorption sites.[26]

Fig. 13, *b* shows that, with all other factors maintained constant, increasing the temperature from 15 °C to 35 °C positively impacted the AE % of *S*-compound from the commercial gasoline. As the process temperature rises, the gasoline's viscosity drops, allowing the adsorbent particles and *S*-compounds to collide more effectively, improving the elimination performance of the *S*-compound from the sample. The AE % of *S*-compound from the viable petrol specimens decreased beyond 30 °C (the typical temperature). This could be because, at higher temperatures, the attractive forces between the adsorbent particles and the *S*-species are reduced, causing a decline in the performance of *S*-compound elimination from commercial fuel.[35,40]

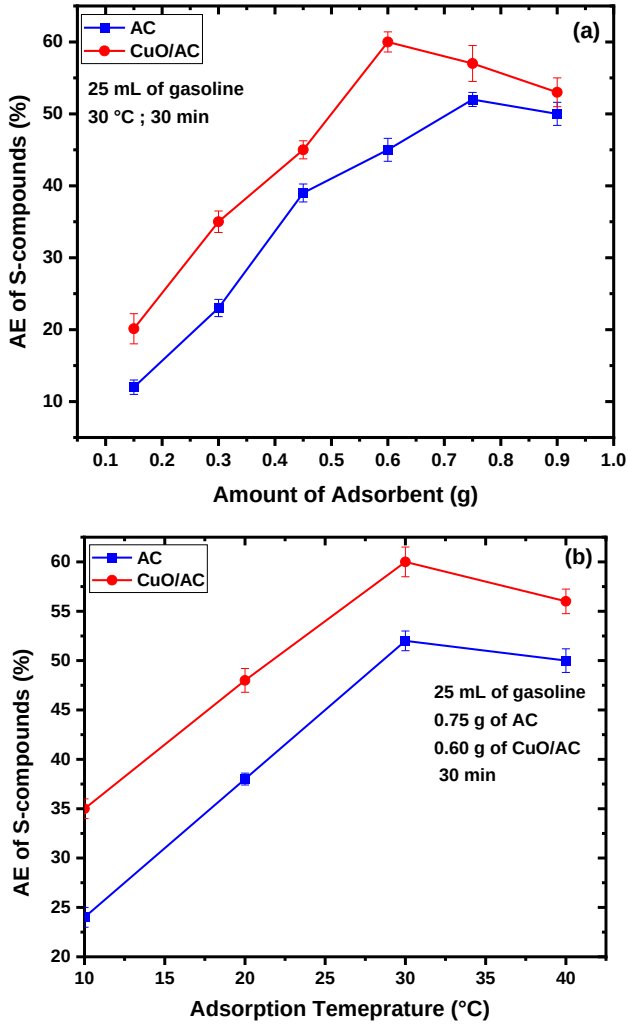

Fig. 13. Effect of conditions on the AE % of *S*-compounds from real fuel

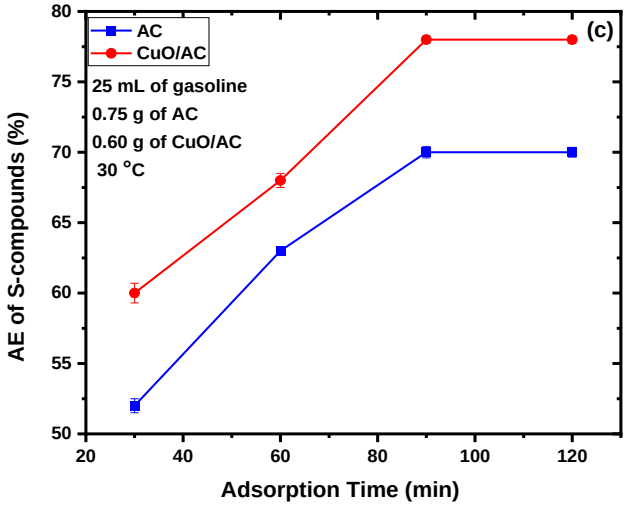

Fig. 13. (Continuation) Effect of conditions on the AE % of *S*-compounds from real fuel

Several trials were conducted over varying durations (30–160 min) while holding all other variables constant to evaluate the impact of the AE % period on *S*-compound removal from commercial fuel. From Fig. 13, *c*, it can be seen that increasing the AE % period improved *S*-compound removal from commercial petrol up to 120 minutes, after which longer durations had little effect because the system had reached equilibrium.

Based on the above results, it appears that the ideal working conditions that led to achieving maximum elimination of DBT from the model using both adsorbents were insufficient to accomplish the greatest exclusion of *S*-compounds from real oil. As such, stringent conditions were needed to reach this target, likely because commercial petrol contains other complex isomers of DBT, such as 2-MDBT, 2,4,6-Tri-DMDBT, 4-MDBT, 2,4-DMDBT, and 4,6-DMDBT.[4] The steric hindrance from side alkyl groups in these compounds makes them more difficult to remove, thereby diminishing removal efficiency. So, it's more difficult to remove these isomers, and harsher conditions could be needed to do it.[2,4,35,40]

3.7. The DS Performance of the Developed Adsorbents Compared with Other

The Q_m values for DBT adsorption by the ABC and its generated nanocomposite in comparison with those declared for other adsorbents in the literature are tabulated in Table 4. The outcomes demonstrated that the developed adsorbents exhibited much higher Q_m values for DBT than previously reported adsorbents. In general, the adsorbents synthesized here for the ADS are promising candidates for the eradication of DBT from liquid oils. The elevated Q_m of the as-generated adsorbents could be attributed to the elevated surface area of the resulting ABC and its derived nanocomposite. Also, effective sites available on the ABC and its developed nanocomposite play an essential role during the adsorption process of *S*-compounds besides pore filling, as these energetic functional groups will aid in the elimination of *S*-species from the oil *via* several auxiliary mechanisms, which afford more adsorption positions to eradicate more species of DBT from the oils. Lastly, the nano diameters of the resulting adsorbents could be more suitable for the adsorption of DBT by carbon-based adsorbents, as the as-prepared adsorbents exhibited a microporous structure, which is characterized by a diameter <2.0 nm, which is suitable for the adsorption of the DBT molecule, which possesses a diameter of 0.80 nm, as reported by Alhamed and Bamufleh.[42] Also, the type of model and solvent used to prepare the models may affect the adsorbents' adsorptive capacity.

Table 4. The Q_m values for DBT adsorption by the developed adsorbents in comparison with those of other adsorbents

Adsorbent	Q_m, mg/g	Ref.
AC from date stones	42.56	[42]
AC	42.0	[43]
AC-N-Mo	48.8	[44]
Microwave-CNT	80.39	[45]
Microwave-CNF	70.38	[45]
Fe_3O_4@MnO_2-w	90.01	[46]
AC	104.56	This study
CuO/AC	117.17	This study

3.8. Mechanism of DBT Removal by Developed Adsorbents

Bonds formation (chemisorption) or physical interactions (*e. g.*, electrostatic forces or dispersion forces) are among the mechanisms by which adsorption occurs on a solid surface[4]. It was established that in physisorption, *S*-compounds remain unchanged.[4,42] Chemisorption links the S atom to the adsorbent's reactive functional group. Multiple mechanisms can cause DBT adsorption on ABC, like the cumulative interactions between the π-systems of the ABC basal planes and the aromatic rings of the DBT molecule.[42] Pearson's hard-soft acid-base concept, which outlines the Lewis acid-base interaction, may also be involved in the adsorption of DBT by AC. At last, formations of complexes between some metal cations with π-electron clouds could also occur.[42,43] The adsorption outcomes disclosed that the inclusion of Cu(II) centers improves desulfurization efficacy. It was established that

chemical adsorption through Lewis acid-base interactions could proceed between DBT species and Cu(II) inside the CuO/AC system.[28] On the other hand, another type of adsorption might be physisorption of DBT *via* π-π stacking interactions between the thiophenic ring of DBT and the as-developed adsorbents. The S atom in DBT molecules owns a lone pair of electrons, which delocalizes π-electrons from aromatic rings across the cyclic structure. This allows π-complexation of DBT-Cu by forming a bond with the unfilled *S*-orbitals of Cu. The π-electron cloud of DBT may serve as an *n*-type or π-type donor by donating its lone pair or delocalizing its π-electrons. Nonetheless, other energetic positions, such as van der Waals interactions, electronic defect centers, and Lewis acidic sites, may also contribute to adsorption.[28,33] Fig. 14 shows the proposed mechanism for DBT exclusion over the prepared adsorbents.[33]

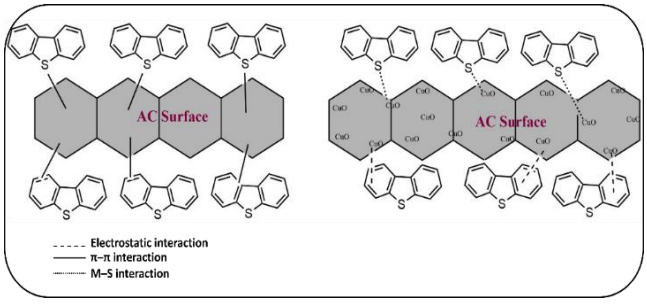

Fig. 14. Suggested mechanism for DBT elimination by the AC and CuO/AC nanocomposite

3.9. Recycling Performance of the Adsorbents

The spent ABC and CuO/ABC nanocomposite were reactivated to verify their effectiveness in the AE of DBT from the model after regeneration and reuse over many cycles.

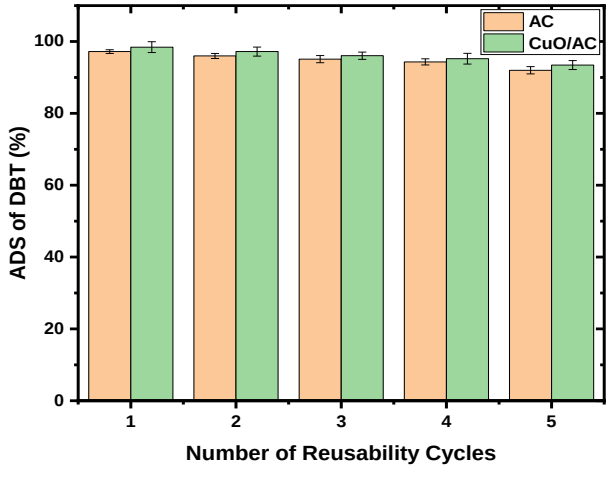

Fig. 15. Reusability cycles of the exhausted adsorbents

Regenerating the exhausted adsorbents was accomplished following the steps described in section 2.5, which included stripping the adsorbed DBT species in a Soxhlet apparatus using *n*-hexane as the solvent, followed by drying and activation for 30 minutes at 500 °C to completely remove the adsorbed DBT. The refreshed adsorbents were repeatedly evaluated for DBT adsorption under specified conditions, followed by regeneration. Fig. 15 displays the AE % of DBT by the adsorbents after each cycle. The ABC and CuO/ABC showed an insignificant decrease in DBT elimination after 6 consecutive reuse runs, indicating their extreme stability under the applied conditions. The modest reduction in DBT eradication capability could be related to slight structural changes or a decrease in the number of active positions upon regeneration.[4,33] The ABC and its developed nanocomposite exhibited high DS performance (90 %) even after several reuse trials, making them cost-effective adsorbents for large-scale fuel oil processing.

4. Conclusions

The present work discusses the development of new ABCs generated from DPs and CuO-ABC nanocomposite adsorbents to eradicate a model oil under mild applied conditions. Characterization using SA_{BET}, XRD, FESEM, and EDX confirmed the successful incorporation of Cu into the ABC, facilitating improved interpretation of the findings. Following the optimized experimental settings of 0.15 g of CuO/ABC nanocomposite, 25 mL of 300 mg/L DBT solution, a reaction period of 25 minutes, and a temperature of 30 ˚C, the removal performance of 99.24 % was achieved, while the highest elimination efficiency (98.09 %) of 25 mL of 300 mg/L DBT solution was achieved 0.20 g of the ABC at 30 ˚C for 25 minutes. The elevated adsorption efficiency and capacity of the CuO/ABC nanocomposite can be attributed to its higher SA_{BET}, which enhances interconnection between Cu and the delocalized π-π electrons of DBT. The adsorption findings closely conformed to the Langmuir adsorption model and agreed with the PSO kinetic model. The adsorbent maintained its activity throughout five consecutive reuses. Due to its cost-effectiveness, ease of operation under moderate conditions, and high efficiency, the current study has significant potential for practical applications in fuel oil processing.

Acknowledgements

We highly acknowledge the support obtainable by Mosul University, College of Science, Chemistry Department.

References

[1] Mohseni, E.; Hamdi, Z.; Parvizimehr, A.; Rahmani, A. Adsorptive Desulphurisation of Benzothiophene and Dibenzothiophene from Model Fuels with Modified Vermiculite. Int. J. Environ. Anal. Chem. 2023, 103, 5691–5705. https://doi.org/10.1080/03067319.2021.1942461
[2] Mohammed-Taib, B. M.; Fadhil, A. B. Dibenzothiophene Capture from Model Fuel by Wild Mustard Stems Derived Activated Carbon: Kinetics and Isothermal Evaluations. Int. J. Environ. Anal. Chem. 2023, 103, 4654–4676. https://doi.org/10.1080/03067319.2021.1931158
[3] Di Gennaro, P.; Franzetti, A.; Bestetti, G.; Lasagni, M.; Pitea, D.; Collina, E. Slurry Phase Bioremediation of PAHs in Industrial Landfill Samples at Laboratory Scale. Waste Manage. 2008, 28, 1338–1345. https://doi.org/10.1016/j.wasman.2007.06.021
[4] Yaseen, M.; Ullah, S.; Ahmad, W.; Subhan, S.; Subhan, F. Fabrication of Zn and Mn Loaded Activated Carbon Derived from Corn Cobs for the Adsorptive Desulfurization of Model and Real Fuel Oils. Fuel 2021, 284, 119102. https://doi.org/10.1016/j.fuel.2020.119102
[5] Ali, I. Sh.; Al-Janabi, O. Y. T.; Al-Tikrity, E. T. B.; Foot, P. J. S. Adsorptive Desulfurization of Model and Real Fuel via Wire-, Rod-, and Flower-Like Fe_3O_4 @MnO_2 @Activated Carbon Made from Palm Kernel Shells as Newly Designed Magnetic Nanoadsorbents. Fuel 2023, 340, 127523. https://doi.org/10.1016/j.fuel.2023.127523
[6] Watanabe, S.; Ma, X.; Song, C. Adsorptive Desulfurization of Jet Fuels over TiO_2 –CeO_2 Mixed Oxides: Role of Surface Ti and Ce Cations. Catal. Today 2021, 371, 265–275. https://doi.org/10.1016/j.cattod.2020.07.071
[7] Betiha, M. A.; Rabie, A. M.; Ahmed, H. S.; Abdelrahman, A. A.; El-Shahat, M. F. Oxidative Desulfurization Using Graphene and Its Composites for Fuel Containing Thiophene and Its Derivatives. Egypt. J. Pet. 2018, 27, 715–730. https://doi.org/10.1016/j.ejpe.2017.10.006
[8] Saha, B.; Vedachalam, S.; Dalai, A. K. Review on Recent Advances in Adsorptive Desulfurization. Fuel Process. Technol. 2021, 214, 106685. https://doi.org/10.1016/j.fuproc.2020.106685
[9] Beshtar, M.; Asgharinezhad, A. A.; Larimi, A. Ultra-Deep Photocatalytic Oxidative Desulfurization of Liquid Fuels by Ti@CeO_2 /ZnO Nanophotocatalyst under Visible Light and Mild Operating Conditions. J. Ind. Eng. Chem. 2024, 134, 548–560. https://doi.org/10.1016/j.jiec.2024.01.017
[10] Pyshyev, S.; Korchak, B.; Miroshnichenko, D.; Vytrykush, N. Influence of Water on Noncatalytic Oxidative Desulfurization of High-Sulfur Straight-Run Oil Fractions. *ACS Omega* **2022**, *7*, 26495−26503. https://doi.org/10.1021/acsomega.2c02527
[11] Yoosuk, B.; Silajan, A.; Prasassarakich, P. Deep Adsorptive Desulfurization over Ion-Exchanged Zeolites: Individual and Simultaneous Effect of Aromatic and Nitrogen Compounds. J. Clean. Prod. 2020, 248, 119291. https://doi.org/10.1016/j.jclepro.2019.119291
[12] Ganiyu, S. A.; Lateef, S. A. Review of Adsorptive Desulfurization Process: Overview of the Non-Carbonaceous Materials, Mechanism and Synthesis Strategies. *Fuel* **2021**, *294*, 120273. https://doi.org/10.1016/j.fuel.2021.120273
[13] Pyshyev, S.; Miroshnichenko, D.; Malik, I.; Contreras, A.B.; N. Hassan; Abd ElRasoul, A. State of the Art in the Production of Charcoal: A Review. *Chem. Chem. Technol*. **2021**, *15*, 61–73. https://doi.org/10.23939/chcht15.01.061
[14] Miroshnichenko, D.; Zhylina, M.; K. Shmeltser. Modern Use of Biochar in Various technologies and Industries: A review. *Chem. Chem. Technol*. **2024**, *18*, 232–243. https://doi.org/10.23939/chcht18.02.232
[15] Zhylina, M; Shishkin, A.; Miroshnichenko, D.; Sterna, V.; Ozolins, J.; Ansone-Bertina, L.; Klavins, M.; Goel, G.; Goel, S. Granulation and Pyrolysis of Agricultural Residues for an Enhanced Circular Economy. *Results Eng*. **2025**, *26*, 104919. https://doi.org/10.1016/j.rineng.2025.104919
[16] Ibrahim, S. Y.; Mahmood, S. F.; Younis, S. A.; Fadhil, A. B. Pyrolysis of Mixed Date Stones and Pistachio Shells: Identification of Bio-Oil and Utilization of Bio-Char as Activated Carbon Precursor. *Chem. Biodiversity* **2023**, *20*, e202300103. https://doi.org/10.1002/cbdv.202300103
[17] Zhang, G.; Zhu, Q.; Zhang, W.; Zheng, Y.; Cao, Y.; Liang, S.; Xiao, Y.; Liu, F.; Jiang, L. Efficiently Integrated Desulfurization from Natural Gas over Zn-ZIF-Derived Hierarchical Lamellar Carbon Frameworks. Inorg. Chem. 2022, 61, 6083–6093. https://doi.org/10.1021/acs.inorgchem.2c00683
[18] Danmaliki, G. I.; Saleh, T. A.; Shamsuddeen, A. A. Response Surface Methodology Optimization of Adsorptive Desulfurization on Nickel/Activated Carbon. Chem. Eng. J. 2017, 313, 993–1003. https://doi.org/10.1016/j.cej.2016.10.136
[19] Saleh, T. A.; Sulaiman, K. O.; Al-Hammadi, S. A.; Dafalla, H.; Danmaliki, G. I. Adsorptive Desulfurization of Thiophene, Benzothiophene and Dibenzothiophene over Activated Carbon Manganese Oxide Nanocomposite: With Column System Evaluation. J. Clean. Prod. 2017, 154, 401–412. https://doi.org/10.1016/j.jclepro.2017.03.219
[20] Adeyi, A.; Abekanmi, F. Comparative Analysis of Adsorptive Desulphurization of Crude Oil by Manganese Dioxide and Zinc Oxide. Res. J. Chem. Sci. 2012, 2, 14–20.
[21] Prajapati, Y. N.; Verma, N. Fixed Bed Adsorptive Desulfurization of Thiophene over Cu/Ni-Dispersed Carbon Nanofiber. Fuel 2018, 216, 381–389. https://doi.org/10.1016/j.fuel.2017.12.046
[22] Naife, T. M. Adsorption Desulfurization of Iraqi Light Naphtha Using Metals Modified Activated Carbon. J. Eng. 2021, 27, 24–41. https://doi.org/10.31026/j.eng.2021.07.03
[23] Nazal, M. K.; Khaled, M.; Atieh, M. A.; Aljundi, I. H.; Oweimreen, G. A.; Abulkibash, A. M. The Nature and Kinetics of the Adsorption of Dibenzothiophene in Model Diesel Fuel on Carbonaceous Materials Loaded with Aluminum Oxide Particles. *Arab. J. Chem.* **2019**, *12*, 3678–3691. https://doi.org/10.1016/j.arabjc.2015.12.003
[24] Xiao, Y.; Fu, J.; Zhu, H.; Zhao, Q.; Zhou, L. Facile and Controllable Preparation of Nanocrystalline ZSM-5 and Ag/ZSM-5 Zeolite with Enhanced Performance of Adsorptive Desulfurization from Fuel. Sep. Purif. Technol. 2022, 288, 120698. https://doi.org/10.1016/j.seppur.2022.120698
[25] Othman, C.S.; Salih, Y.M.; Hamasalih, L.O. Adsorption Desulfurization of Dibenzothiophene in a Model and Diesel Fuel by Hybrid Activated Charcoal/Mixed Metal Oxide. *Pet. Sci. Technol.* 2023, *41*, 2121-2140. https://doi.org/10.1080/10916466.2022.2108052
[26] Abdulhamid, Q. M.; Al-Tikrity, E. T.; Fadhil, A. B.; Foot, P. J. Thermal Cracking of Al-Dora Asphalt for the Simultaneous Production of Light Fuel and Activated Carbon for Desulfurization Process. J. Anal. Appl. Pyrolysis 2023, 173, 106072. https://doi.org/10.1016/j.jaap.2023.106072
[27] Li, G.; Zhang, H.; Chen, Y.; Yang, H.; Chen, H. Preparation and Characterization of the Hydrogen Storage Activated Carbon from Coffee Shell by Microwave Irradiation and KOH Activation. Int. Biodeterior. Biodegrad. 2016, 113, 386–390. https://doi.org/10.1016/j.ibiod.2016.05.003

[28] Yang, Z.; Chen, Z.; Gong, H.; Wang, X. Copper Oxide Modified Activated Carbon for Enhanced Adsorption Performance of Siloxane: An Experimental and DFT Study. Appl. Surf. Sci. 2022, 601, 154200. https://doi.org/10.1016/j.apsusc.2022.154200
[29] Prajapati, Y. N.; Verma, N. Adsorptive Desulfurization of Diesel Oil Using Nickel Nanoparticle-Doped Activated Carbon Beads with/Without Carbon Nanofibers: Effects of Adsorbate Size and Adsorbent Texture. Fuel 2017, 189, 186–194. https://doi.org/10.1016/j.fuel.2016.10.065
[30] Fayazi, M.; Ghanei-Motlagh, M. Enhanced Performance of Adsorptive Removal of Dibenzothiophene from Model Fuel over Copper (II)-Alginate Beads Containing Polyethyleneterephthalate Derived Activated Carbon. J. Colloid Interface Sci. 2021, 604, 517–525. https://doi.org/10.1016/j.jcis.2021.06.097
[31] Zhou, K.; Ma, W.; Zeng, Z.; Xu, X.; Liu, B.; Li, H.; Li, L. Waste Biomass-Derived Oxygen and Nitrogen Co-Doped Porous Carbon/MgO Composites as Superior Acetone Adsorbent: Experimental and DFT Study on the Adsorption Behavior. Chem. Eng. J. 2020, 387, 124173. https://doi.org/10.1016/j.cej.2019.124173
[32] Peternela, J.; Silva, M. F.; Vieira, M. F.; Bergamasco, R.; Marquetotti Salcedo Vieira, A. Synthesis and Impregnation of Copper Oxide Nanoparticles on Activated Carbon through Green Synthesis for Water Pollutant Removal. Mater. Res. 2017, 21, e20160460. https://doi.org/10.1590/1980-5373-MR-2016-0460
[33] Rao, V. D.; Rao, M. V. S.; Krishna, M. M. Chromium (VI) Removal Using Activated Thuja occidentalis Leaves Carbon Powder – Adsorption Isotherms and Kinetic Studies. Chem. Chem. Technol. 2020, 14, 362–371. https://doi.org/10.23939/chcht14.03.362
[34] Zhang, P.; O'Connor, D.; Wang, Y.; Jiang, L.; Xia, T.; Wang, L.; Tsang, D. C. W.; Ok, Y. S.; Hou, D. A Green Biochar/Iron Oxide Composite for Methylene Blue Removal. J. Hazard. Mater. 2020, 384, 121280. https://doi.org/10.1016/j.jhazmat.2019.121280
[35] Nayyef, W. A.; Fadhil, A. B. Elimination of Dibenzothiophene from Model Gasoline by Binary Biowastes-Derived Activated Carbon. Chem. Eng. Technol. 2023, 46, 681–693. https://doi.org/10.1002/ceat.202200463
[36] Mahmood, Q. A.; Humadi, J. I.; Algawi, R. J.; Nawaf, A. T.; Ahmed, I. A. Adsorption Desulfurization of Simulated Diesel Fuel Using Graphene Oxide. Chem. Chem. Technol. 2024, 18, 436–441. https://doi.org/10.23939/chcht18.03.436
[37] Tang, C.; Shu, Y.; Zhang, R.; Li, X.; Song, J.; Li, B.; Zhang, Y.; Ou, D. Comparison of the Removal and Adsorption Mechanisms of Cadmium and Lead from Aqueous Solution by Activated Carbons Prepared from Typha angustifolia and Salix matsudana. RSC Adv. 2017, 7, 9224–9236. https://doi.org/10.1039/C6RA28035H
[38] Olajire, A. A.; Olanrewaju, S. A.; Lawal, W. H. Silver Nanoparticle-Assisted Adsorptive Desulfurization by Composted Agro-Waste Activated Carbons. Int. J. Environ. Res. 2017, 11, 263–279.
[39] Gorzin, F.; Bahri Rasht Abadi, M. M. Adsorption of Cr(VI) from Aqueous Solution by Adsorbent Prepared from Paper Mill Sludge: Kinetics and Thermodynamics Studies. Adsorpt. Sci. Technol. 2018, 36, 149–169. https://doi.org/10.1177/0263617416686976
[40] Hussein, A. A. Kinetics and Isothermal Evaluations of Adsorptive Desulfurization of Dibenzothiophene over Mixed Bio-Wastes Derived Activated Carbon. Energy Sources, Part A: Recovery, Utilization, and Environmental Effects 2021, 43, 2840–2859. https://doi.org/10.1080/15567036.2021.1878430
[41] Can, N. Electrospun CuO Nanofibers for Room Temperature Volatile Organic Compound Sensing Applications. Mater. Chem. Phys. 2018, 212, 377–384. https://doi.org/10.1016/j.matchemphys.2018.03.069
[42] Alhamed, Y. A.; Bamufleh, H. S. Sulfur Removal from Model Diesel Fuel using Granular Activated Aarbon from Dates' Stones Activated by $ZnCl_2$. *Fuel* **2009**, *88*, 87–94. https://doi.org/10.1016/j.fuel.2008.07.019
[43] Saleh, T. A.; Danmaliki, G. I. Adsorptive Desulfurization of Dibenzothiophene from Fuels by Rubber Tyres-Derived Carbons: Kinetics and Isotherms Evaluation. Process Saf. Environ. Prot. 2016, 102, 9–19. https://doi.org/10.1016/j.psep.2016.02.023
[44] Azeez, M. O.; Tanimu, A.; Alhooshani, Kh.; Ganiyu, S. A. Synergistic Effect of Nitrogen and Molybdenum on Activated Carbon Matrix for Selective Adsorptive Desulfurization: Insights into Surface Chemistry Modification. *Arab. J. Chem.* **2022**, *15*, 103454. https://doi.org/10.1016/j.arabjc.2021.103454
[45] Jha, D.; Mubarak, N. M.; Haider, M. B.; Kumar, R.; Balathanigaimani, M. S.; Sahu, J. N. Adsorptive Removal of Dibenzothiophene from Diesel Fuel Using Microwave Synthesized Carbon Nanomaterials. Fuel 2019, 244, 132–139.

Received: July 11, 2025 / Revised: November 21, 2025 / Accepted: December 10, 2025

СИНТЕЗ ФУНКЦІОНАЛІЗОВАНОГО НАНООКСИДОМ МІДІ МІКРОПОРИСТОГО АКТИВОВАНОГО БІОВУГІЛЛЯ, ОТРИМАНОГО З КІСТОЧОК ФІНІКІВ, ТА ЙОГО ЗАСТОСУВАННЯ В АДСОРБЦІЙНІЙ ДЕСУЛЬФУРАЦІЇ МОДЕЛЬНИХ ТА РЕАЛЬНИХ МАСТИЛ

Анотація. *Вивчено синтез активованого біовугілля (ABC) з кісточок фініків та нанокомпозиту CuO-ABC для адсорбційної елімінації (АЕ) модельних та комерційних палив. Результати, отримані за допомогою FESEM, TEM, EDX, XRD та ізотерм адсорбції–десорбції N_2, підтвердили мікропористу структуру обох адсорбентів. SA_{BET} та діаметр пор ABC становили відповідно 765,52 $м^2/г$ та 1,79 нм, тоді як SA_{BET} та діаметр пор нанокомпозиту CuO-ABC відповідно 621,57 $м^2/г$ та 1,99 нм, що вказує на мікропористі структури обох адсорбентів. Максимальний АЕ % 200 мг/л розчину DBT за допомогою ABC становив 98,09 % у разі використання 0,20 г ABC за 30 °C протягом 25 хв. Для порівняння, найвищий АЕ % 200 мг/л розчину DBT над нанокомпозитом CuO-ABC становив 99,24 %, досягнутий із використанням 0,15 г нанокомпозиту за 30 °C упродовж 20 хв. Ізотермічні та кінетичні дослідження показали, що ізотерма адсорбції Ленгмюра та кінетична модель псевдодругого порядку найкраще описують адсорбцію DBT. Обидва адсорбенти продемонстрували стійку активність протягом п'яти послідовних циклів. Вміст сірки в реальному бензині знизився до 80,12 % і 84,22 % після використання 0,60 г обох адсорбентів за 30 °C протягом 120 хв. У роботі запропоновано економічно ефективні адсорбенти для десульфурації модельної системи десульфурації та реальних паливних мастил у промислових масштабах.*

Ключові слова: *кісточки фініків, активоване біовугілля, нанокомпозит CuO/ABC, адсорбційна елімінація DBT, ізотерма та кінетика адсорбції.*